INORGANIC CHEMISTRY
FRONTIERS

RESEARCH ARTICLE

View Article Online
View Journal

Cite this: DOI: 10.1039/d6qi00095a

Substituent effects on *o*-carborane reactivity with cyclic (alkyl)(amino)carbenes

Nardeen Safadi, Vladimir Kampel and Roman Dobrovetsky *

The functionalization of carboranes, particularly at boron vertices, is a topic of extensive research. Here, we report the reactivity of *ortho*-carboranes (***o*Cb**s) with cyclic (alkyl)(amino)carbenes (CAACs) – a transformation that, surprisingly, has not been previously reported. We found that the substitution at the carbon atoms of an ***o*Cb** strongly influences the reaction outcome. An unsubstituted ***o*Cb** (H at carbon) reacts with the CAAC *via* carbene insertion into the C–H bond. However, when the carbon atoms of the ***o*Cb** are substituted, the reaction is dictated by the electronic nature of these substituents: electron-withdrawing groups (EWGs) promote the formation of *nido*-type products *via* the nucleophilic attack by the CAAC at the B3 (or B6) position, whereas electron-donating groups (EDGs) favor insertion of the CAAC into the B–H bonds at these positions. The explanation of this reactivity pattern, along with the proposed mechanism of these processes, is supported experimentally and by density functional theory (DFT) computations.

Received 14th January 2026,
Accepted 27th February 2026

DOI: 10.1039/d6qi00095a

rsc.li/frontiers-inorganic

Introduction

Carboranes have been known since the 1950s,[1] and have since found applications in various fields. For example, they enhance the heat resistance and hydrophobicity of polymers,[2] play a role in boron neutron capture therapy in medicine,[2,3] are used for electrochemical energy storage,[4,5] serve as ligand building blocks in catalyst design,[6–8] aid in metal recovery from radioactive waste,[9–11] and function as weakly coordinating anions.[12,13]

ortho-Carboranes (***o*Cb**s) have gained significant attention in recent decades due to their unique features, such as non-classical carbon–boron and boron–boron bonds that are stabilized by σ-electron delocalization in the cluster. This electron delocalization is referred to as 3D aromaticity, in analogy to the 2D aromaticity of benzene rings, and similarly contributes to the stabilization of the cluster.[14,15]

The two carbon atoms in ***o*Cb**s alter the electronic properties of both the endo- and exoskeleton frameworks.[16,17] The functionalization of exoskeleton C–H and B–H bonds is key to the modification and use of this cluster in synthetic chemistry.[18,19] The C–H units in ***o*Cb**s are acidic and susceptible to deprotonation by Brønsted bases such as ^{n}BuLi, KHMDS, *etc*.[20–23] Once deprotonated, the ***o*Cb**s can be further modified by installing various functional groups.[24–27,28] In contrast, the high s-character of the sp hybridized B atoms at the vertices increases their effective electronegativity, making the exoskeleton B–H bonds nearly nonpolar and therefore only weakly hydritic.[25,29,30] Consequently, functionalizing the B atoms in ***o*Cb**s is more challenging.

Earlier work on ***o*Cb** functionalization showed that the direct functionalization of cage B–H vertices in ***o*Cb**s could be achieved *via* electrophilic substitution with various electrophiles under forced reaction conditions.[31–34] This approach was typically limited to substitution at the B(9,12)–H bonds, as these positions are the most electron-rich in ***o*Cb**s.[35] The direct regioselective functionalization of other B–H vertices became possible with transition metal-catalyzed cross-coupling reactions, primarily employing noble metals such as Pd, Ir, Rh, and Ru, often facilitated by a directing group installed on ***o*Cb**s.[36–38] Xie reported numerous examples of this chemistry over the years, introducing highly selective and efficient methods for B-functionalization in ***o*Cb**s.[32,36–43] More recently, Xie has reported a series of impressive transition-metal-free strategies for direct B–H functionalization using Grignard reagents[44] and magnesium bisamides.[45]

We became interested in the chemistry of ***o*Cb**s with carbenes, as carbenes have been shown to react with both C–H and B–H vertices. In 1983, Jones Jr. reported the reaction between an ***o*Cb** and carboethoxycarbene, an unstable singlet carbene formed *in situ* from the corresponding diazo compound,[46] which yielded a mixture of four isomers resulting from carbene insertion into B–H bonds.[47,48] Notably, Lee recently reported an impressive Rh(II)-catalyzed site- and enantioselective B–H insertion reaction using singlet carbenes.[49] With the development of stable N-heterocyclic car-

School of Chemistry, Raymond and Beverly Sackler Faculty of Exact Sciences, Tel Aviv University, Tel Aviv 69978, Israel. E-mail: rdobrove@tau.ac.il

benes (NHCs), their reactivity with ***o*Cb**s was also studied. Smaller NHCs primarily acted as Brønsted bases, deprotonating the C–H bonds in ***o*Cb**s,[50] while bulkier NHCs functioned as Lewis bases, attacking the most electrophilic boron centre (B3 or B6) and opening the cluster to a *nido*-type structure.[51,52]

Surprisingly, the reactivity of cyclic (alkyl)(amino)carbenes (CAACs), which are both stronger σ-donors and better π-acceptors, with ***o*Cb**s has not been reported.[53] We envisioned that the ambiphilicity of CAACs could lead to distinct reactivity patterns with ***o*Cb**s, and decided to take on this task to fill this gap in the reactivity of carbenes and ***o*Cb**s. In this paper, we present the reactivity of ^{Me2}**CAAC**[54] with ***o*Cb**s bearing different substituents at the carbon atoms (H, electron-withdrawing groups (EWGs), and electron-donating groups (EDGs)), demonstrating that these substituents play a crucial role in determining the reaction outcome. The mechanism, supported by both experiments and DFT calculations, explaining these distinct reactivities is also presented.

Results and discussion

First, the reaction between ^{Me2}**CAAC** and an equimolar amount of ***o*Cb** was carried out in benzene at room temperature. The ^{13}C-NMR spectrum recorded after 12 h showed the disappearance of the carbene carbon signal (δ = 312 ppm), indicating complete consumption of ^{Me2}**CAAC**. Analysis of the ^{1}H, ^{13}C, and ^{11}B NMR spectra revealed that the reaction process was neither a mere deprotonation, a nucleophilic attack on the B atoms, nor an insertion into the B–H bond of the ***o*Cb**, as previously reported for carbene reactions.[46–48,50–52] Instead, the NMR data suggested a carbene insertion into the C–H bond, yielding product **1** (Fig. 1), a reactivity that, to the best of our knowledge, has not been previously reported. Evaporation of volatiles under vacuum afforded a yellowish precipitate, which was washed with pentane. Crystallization from benzene yielded transparent crystals, and single-crystal X-ray diffraction (SC-XRD) confirmed the molecular structure as insertion product **1** (Fig. 2).

We propose that the formation of **1** starts with the deprotonation of the ***o*Cb** by ^{Me2}**CAAC**, which acts as a Brønsted base. This deprotonation generates an intermediate salt consisting

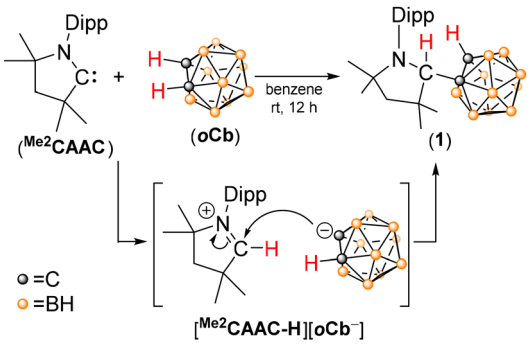

Fig. 1 ^{Me2}**CAAC** insertion into the C–H bond of ***o*Cb**.

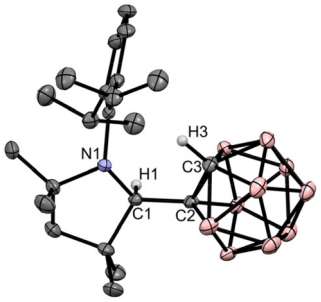

Fig. 2 POV-ray depiction of **1**. Thermal ellipsoids at 30% probability, and non-relevant hydrogen atoms are omitted for clarity.

of the cyclic iminium cation [^{Me2}**CAAC-H**]$^{+}$ and the carboranyl anion ***o*Cb**$^{-}$ (Fig. 1). This assumption is supported by previous reports on NHC reactions with ***o*Cb**s, where NHCs similarly acted as Brønsted bases.[50] However, unlike imidazolium cations, [NHC-H]$^{+}$, which are poor electrophiles, the cyclic iminium [^{Me2}**CAAC-H**]$^{+}$ is a significantly better electrophile. As a result, it undergoes nucleophilic attack by ***o*Cb**$^{-}$, leading to the formation of the insertion product **1** (Fig. 1).

As mentioned above, unstable singlet carbenes can react with ***o*Cb**s to yield the B–H insertion products,[47,48] while NHCs react with ***o*Cb**s, attacking the B3 (or B6) atom, leading to *nido*-type products.[51,52] This suggests that ^{Me2}**CAAC** might exhibit similar reactivity. However, achieving these transformations would require replacing the hydrogen atoms on the carbon atoms of ***o*Cb**s with non-reactive "protecting" groups.

Thus, to force the reactivity with the B–H vertices, first dimethyl carborane (^{Me2}***o*Cb**) was synthesized[55] and reacted with ^{Me2}**CAAC** (1 : 1) in benzene at rt (Fig. 3). After 12 h, NMR spectra were recorded, showing the disappearance of the carbene carbon signal in the ^{13}C NMR spectrum (δ = 312 ppm), and the appearance of new signals at δ = 3.07 ppm in the ^{1}H NMR spectrum and at δ = 63.17 and 62.43 ppm in the ^{13}C NMR spectrum, which were attributed to the N–**C**–**H** fragment of the pyrrolidine type moiety that originated from the ^{Me2}**CAAC**, which was further confirmed by heteronuclear single quantum coherence (HSQC) NMR. Finally, the obtained product was crystallized from benzene, and its molecular structure was determined by SC-XRD (Fig. 4) as the product of the double insertion of ^{Me2}**CAAC** into the B–H bonds at the B3 and B6 positions (**2**^{clscls}) (Fig. 3).

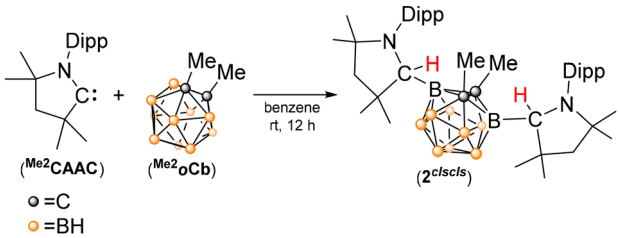

Fig. 3 ^{Me2}**CAAC** insertion into the B–H bonds of ^{Me2}***o*Cb**.

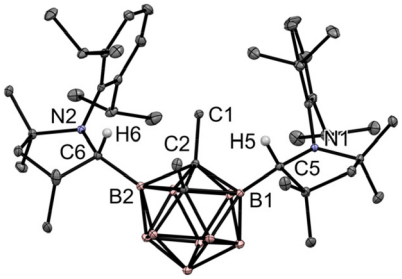

Fig. 4 POV-ray depiction of $\mathbf{2}^{clscls}$. Thermal ellipsoids at 30% probability, and non-relevant hydrogen atoms are omitted for clarity.

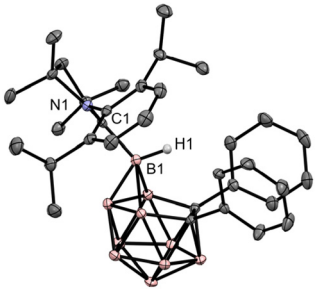

Fig. 6 POV-ray depiction of $\mathbf{3}^{nido}$. Thermal ellipsoids at 30% probability, and non-relevant hydrogen atoms are omitted for clarity.

It is important to note that even when an excess of ^{Me2}***o*Cb** (3 : 1) was used to prevent double insertion and favour the 1 : 1 reaction, the outcome remained the same, yielding product $\mathbf{2}^{clscls}$. Interestingly, unlike the previously reported reaction between ***o*Cb** and bulky NHCs, where the carbene attacked the B-centre leading to a *nido* cluster,[52] ^{Me2}**CAAC** reacted with ^{Me2}***o*Cb** similarly to unstable carbenes, *i.e.*, *via* B–H insertion,[47,48] but in a more selective manner.

We assumed that replacing the two methyl groups in ^{Me2}***o*Cb** with bulkier substituents at the carbon atoms of the ***o*Cb** cluster could prevent double insertion and yield a 1 : 1 product. To test this hypothesis, ^{Ph2}***o*Cb** was prepared[56] and reacted with ^{Me2}**CAAC**, leading after 12 h to a 1 : 1 product resulting from ^{Me2}**CAAC** attack at the B3 atom of ^{Ph2}***o*Cb**, forming *nido* carborane $\mathbf{3}^{nido}$ (Fig. 5) rather than the expected B–H insertion product. $\mathbf{3}^{nido}$ was crystallized from CH_2Cl_2 as colorless crystals, and its structure was determined by SC-XRD (Fig. 6).

Notably, the reaction of ^{Ph2}***o*Cb** with ^{Me2}**CAAC**, which leads to the *nido* product $\mathbf{3}^{nido}$ (Fig. 5), resembles the previously reported reaction of bulky NHCs with ***o*Cb**s.[51] However, it differs significantly from the reaction of ^{Me2}**CAAC** with ^{Me2}***o*Cb** (Fig. 3). This contrast highlights the strong dependence of these reactions on the steric and electronic properties of the substituents at the carbon centres of the ***o*Cb**. The Me groups are σ-donating, while the Ph groups are π-donating and σ-withdrawing.

We propose that the B–H insertion product $\mathbf{2}^{cls}$ is formed *via* *nido*-type intermediate $\mathbf{2}^{nido}$ (Fig. 7), structurally similar to $\mathbf{3}^{nido}$, which is formed as a result of an attack of ^{Me2}**CAAC** at

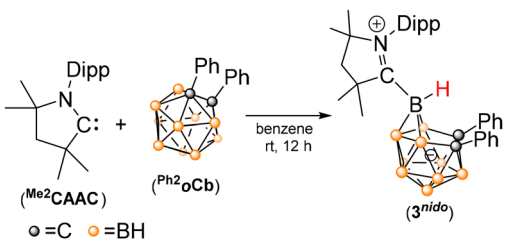

Fig. 5 Reaction of ^{Me2}**CAAC** and ^{Ph2}***o*Cb** – formation of the *nido*-type product $\mathbf{3}^{nido}$.

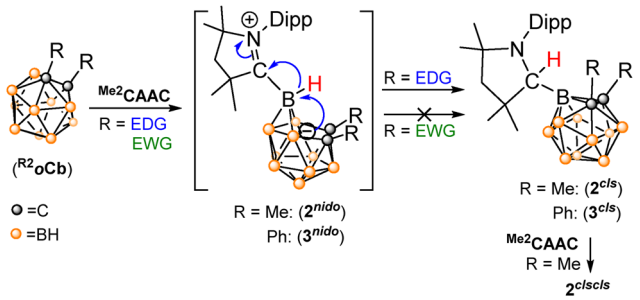

Fig. 7 Proposed pathway for B–H insertion and the influence of the substituents (EWG *vs.* EDG) on the reaction outcome.

the most electrophilic B3 (or B6) atom of the ^{Me2}***o*Cb**. A subsequent hydride migration from the B–H moiety in $\mathbf{2}^{nido}$ to the cyclic iminium unit closes the cluster, yielding $\mathbf{2}^{cls}$. A similar reaction sequence with the second molecule of ^{Me2}**CAAC** ultimately leads to the formation of product $\mathbf{2}^{clscls}$ (Fig. 7).

It is noteworthy that while the attack of NHCs on the B-centres of ***o*Cb**s, leading to *nido* carboranes, is well-documented, the subsequent hydride migration and cluster closure have not been reported and are actually rather rare phenomena in carboranes in general.[29,30,57,58] This difference likely stems from the distinct electronic properties of CAACs and NHCs. CAACs are more ambiphilic than NHCs, and after the formation of $\mathbf{2}^{nido}$, the iminium moiety becomes highly electrophilic, making it capable of accepting a hydride from the adjacent B–H unit (Fig. 7). Notably, an alternative mechanism similar to the one proposed for C–H insertion (Fig. 1) can be ruled out, as the hydrogen atoms at the B-centres of carborane are not acidic.

An obvious question arises: why does the reaction with ^{Ph2}***o*Cb** stop at the *nido*-type compound $\mathbf{3}^{nido}$ and not proceed through hydride migration to the *closo* form? To explain this, we propose that hydride migration from the B-centre to the iminium moiety can be viewed as a nucleophilic substitution-like process. The more electron-rich the *nido* cage, the more favorable this nucleophilic substitution becomes, leading to B–H insertion products (Fig. 7). In contrast, if the *nido* cage is less electron-rich, hydride migration slows down or is entirely inhibited. In other words, when carborane is functionalized

with an electron-donating group (EDG), such as methyl, the *nido* cage becomes more nucleophilic, facilitating hydride migration and cluster closure, ultimately yielding the B–H insertion products. However, if the substituents at the ***o*Cb** are electron-withdrawing groups (EWGs), such as phenyl, the *nido* cage is less electron-rich and lacks sufficient nucleophilicity to promote hydride migration and cluster closure, thus halting the reaction at the *nido* stage (Fig. 7).

Additionally, steric factors may also influence the conversion from the *nido* to the *closo* form. If the structural reorganization required for hydride migration leads to significant steric repulsion between substituents at the carbon centres of the ***o*Cb**, the closure of the cluster may be kinetically hindered or entirely suppressed.

To support this hypothesis, DFT computations of the hydride migration from the boron to a carbon atom, causing the transformation from the *nido*-type carboranes $\mathbf{2}^{nido}$ and $\mathbf{3}^{nido}$ to *closo*-type carboranes $\mathbf{2}^{cls}$ and $\mathbf{3}^{cls}$ (not formed in the reaction), respectively, were performed at the BP86-D3/def2-TZVP level of theory.[59–61] These computational results revealed that the hydride migration in $\mathbf{2}^{nido}$ leading to $\mathbf{2}^{cls}$ is a significantly exothermic (ΔH = −12.4 kcal mol^{-1}) and exergonic (ΔG = −9.7 kcal mol^{-1}) process, proceeding through a reasonable free energy barrier ($\Delta G^{\ddagger}$ = 21.8 kcal mol^{-1}) (Fig. 8, blue). In contrast, the same process for $\mathbf{3}^{nido}$ leading to $\mathbf{3}^{cls}$, which was not observed experimentally, was calculated to be enthalpy and free energy neutral (ΔH = −2.5 and ΔG = −0.7 kcal mol^{-1}) with a free energy barrier of $\Delta G^{\ddagger}$ = 23.1 kcal mol^{-1} (Fig. 8, red).

These computational results suggest that hydride migration in $\mathbf{3}^{nido}$ leading to $\mathbf{3}^{cls}$ should also be observed, and possibly was not observed due to the energy barrier. Consequently, we decided to heat $\mathbf{3}^{nido}$ to force the formation of $\mathbf{3}^{cls}$. Thus, $\mathbf{3}^{nido}$ dissolved in $CDCl_3$ was heated to 60 °C, and the reaction was monitored by NMR spectroscopy. As a result, after 12 h, the ^{1}H NMR spectrum of the reaction mixture showed the emergence of two new septet signals at δ = 3.12 and 4.05 ppm, while the intensity of the septet signal of $\mathbf{3}^{nido}$ at δ = 2.84 ppm decreased. Probably, the reason for obtaining two new signals of septets (that correspond to the hydrogens of $CH(CH_3)_2$) instead of one septet signal as in $\mathbf{3}^{nido}$ is due to the loss of symmetry in the molecule $\mathbf{3}^{cls}$; the hydride migrates to the empty orbital of ^{Me2}**CAAC** and the carbenic carbon becomes sp^3 hybridized (see the SI for more details).

To provide additional experimental evidence for our hypothesis, we synthesized ^{pCF3Ph2}***o*Cb** with an electron-withdrawing substituent at the carbon atoms of the ***o*Cb**, as well as a mono-substituted ***o*Cb** bearing a bulky electron-withdrawing *ortho*-carboranyl substituent, ^{oCb}***o*Cb** (biscarborane). Additionally, we prepared ^{pTol2}***o*Cb**, ^{Anis2}***o*Cb**, and ^{Anil2}***o*Cb**, which contain electron-donating substituents, along with ^{Si}***o*Cb**, substituted with the bulky electron-donating Me$_2$^{t}BuSi-group. These compounds were then reacted with ^{Me2}**CAAC** (Fig. 9).

Thus, ***o*Cb**s with electron-withdrawing groups (EWGs), ^{pCF3Ph2}***o*Cb** and ^{oCb}***o*Cb**, reacted with ^{Me2}**CAAC** at r.t., leading to adduct formation and *nido*-type carboranes $\mathbf{4}^{nido}$ and $\mathbf{5}^{nido}$ (Fig. 9, path a). Interestingly, no deprotonation occurred despite the presence of protic C–H moieties in ^{oCb}***o*Cb**. This suggests that either the *ortho*-carboranyl substituent provides sufficient steric protection to prevent deprotonation or its electronic effects favour nucleophilic attack at the B3 (or B6) centre. Notably, Peryshkov observed similar reactivity for the biscarboranylphosphine compound in the reaction with phosphines.[62] Both $\mathbf{4}^{nido}$ and $\mathbf{5}^{nido}$ were crystallized, and their molecular structures were determined by SC-XRD (Fig. 10).

Importantly, heating $\mathbf{4}^{nido}$ and $\mathbf{5}^{nido}$ in $CDCl_3$ to 80 °C for 12 h did not lead to any observable changes in the NMR spectra, indicating that no hydride migration and transformation to *closo* carboranes occur in these cases (Fig. 9, path b).

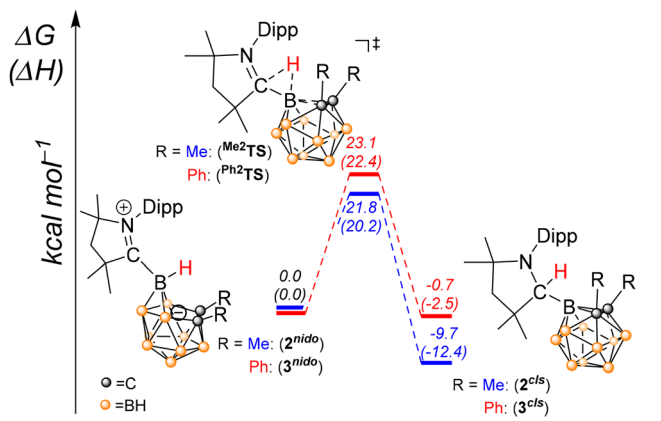

Fig. 8 DFT computed mechanism of the hydride migration from the boron to the carbon atom, producing from the *nido*-type compounds $\mathbf{2}^{nido}$ and $\mathbf{3}^{nido}$ *closo*-type carboranes $\mathbf{2}^{cls}$ and $\mathbf{3}^{cls}$, respectively.

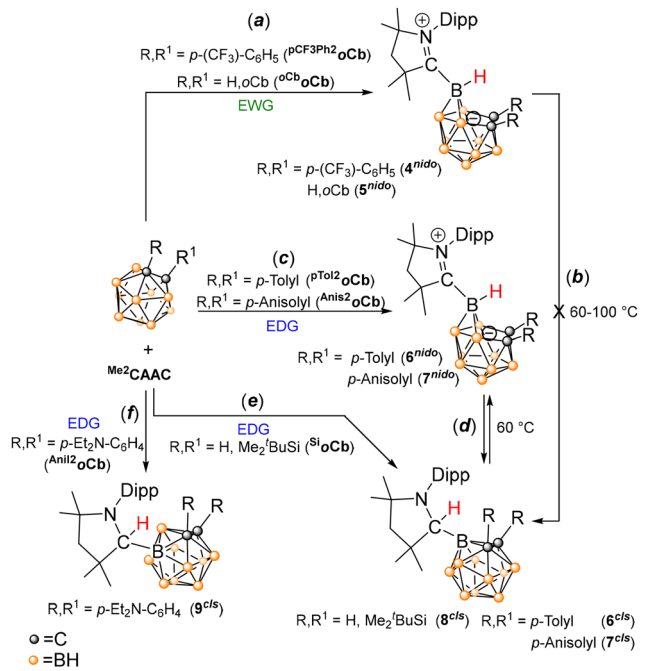

Fig. 9 Reactions of ^{Me2}**CAAC** with ^{pTol2}***o*Cb**, ^{Anis2}***o*Cb**, ^{Anil2}***o*Cb**, ^{pCF3Ph}$_2$***o*Cb**, ^{Si}***o*Cb**, and ^{oCb}***o*Cb**.

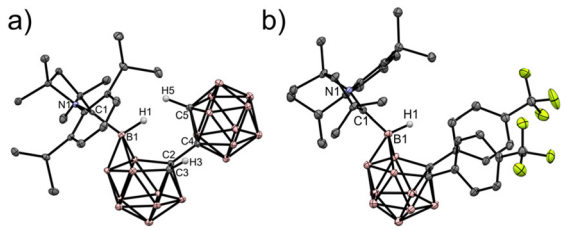

Fig. 10 POV-ray depiction of 4^{nido} (a) and 5^{nido} (b). Thermal ellipsoids at 30% probability, and non-relevant hydrogen atoms are omitted for clarity.

This supports our mechanistic suggestion that in ***o*Cb**s with EWG substituents at the carbon atom(s), this transformation is precluded due to the low nucleophilicity of the *nido*-type open cluster. This is also supported by the DFT calculations (BP86-D3/def2-TZVP)[59–61] done for the hydride migration and transformation to *closo* carboranes for both 4^{nido} and 5^{nido}. For both compounds, 4^{nido} and 5^{nido}, this process was computed to be mildly endergonic (ΔG = 2.5 and 4.0 kcal mol^{-1}, respectively) (see Fig. 12, red and blue).

The ***o*Cb**s with EDGs, ^{pTol2}***o*Cb**, and ^{Anis2}***o*Cb**, reacted with ^{Me2}**CAAC** at r.t., leading to *nido*-type carboranes 6^{nido} and 7^{nido}, respectively (Fig. 9, path c). The molecular structures of both compounds were determined by SC-XRD (Fig. 11). In contrast to 4^{nido} and 5^{nido}, heating of which did not lead to any observable change, heating 6^{nido} and 7^{nido} in $CDCl_3$ at 60 °C after 12 h led to clearly observable changes in the NMR spectra (see the SI for details), which were attributed to hydride migration and the closing of the cluster to *closo* forms 6^{cls} and 7^{cls}, respectively (Fig. 9, path d). In both cases, the reaction of ^{pTol2}***o*Cb** and ^{Anis2}***o*Cb** with ^{Me2}**CAAC**, the products of hydride migration and the closing of the *nido* carborane, 6^{cls} and 7^{cls}, respectively, were isolated by washing the crude solid with hexane, followed by crystallization from hexane. The molecular structures of 6^{cls} and 7^{cls} were determined by SC-XRD (Fig. 11). This again supports the suggested mechanism for this process, which is also supported by DFT calculations (BP86-D3/def2-TZVP)[59–61] that showed that in both cases the transformation from 6^{nido} and 7^{nido} to 6^{cls} and 7^{cls}, respectively, is exergonic (ΔG = −0.8 and −3.0 kcal mol^{-1}, respectively) (Fig. 12, brown and green).

The ^{Si}***o*Cb** was reacted with ^{Me2}**CAAC** in benzene (1 : 1) at r.t. However, NMR spectra recorded after 12 h indicated that no reaction occurred. Therefore, the reaction was heated to 80 °C, which led to an observable change in the ^{1}H NMR spectra after 6 h, which revealed that ^{Si}***o*Cb** and ^{Me2}**CAAC** had been fully consumed. Upon slow evaporation of benzene, crystals were formed, and their molecular structure was determined by SC-XRD as a 1 : 1 product of ^{Me2}**CAAC** insertion into the B3–H bond, product 8^{cls} (Fig. 9, path e; see Fig. 13a for the X-ray molecular structure of 8^{cls}). This result is also supported by DFT computations (BP86-D3/def2-TZVP),[59–61] which show that the conversion from the *nido*-type carborane 8^{nido} to 8^{cls} is strongly exergonic (ΔG = −7.7 kcal mol^{-1}) (Fig. 12, purple).

Notably, 8^{nido} was not observed in this reaction under these reaction conditions, which can be explained by the thermodynamics of the hydride migration, favouring the formation of 8^{cls}. Importantly, the obtained product 8^{cls} indicates that the ^{t}BuMe$_2$Si substituent was sufficiently bulky to prevent the reaction of ^{Me2}**CAAC** with the C–H bond of the ^{Si}***o*Cb**. Furthermore, the obtained reaction was selective, and only one insertion occurred, which contrasts with the reaction of ^{Me2}***o*Cb** with ^{Me2}**CAAC**, which reacted 1 : 2, respectively, leading to 2^{clscls} (Fig. 3), which can be attributed to the steric factor in ^{Si}***o*Cb** *vs.* ^{Me2}***o*Cb**, with the former being significantly bulkier.

Interestingly, the reaction of ^{Anil2}***o*Cb** with ^{Me2}**CAAC** in C_6D_6 did not produce any result at r.t.; however, upon prolonged heating at 60 °C for 10 days, it led to the clean formation of

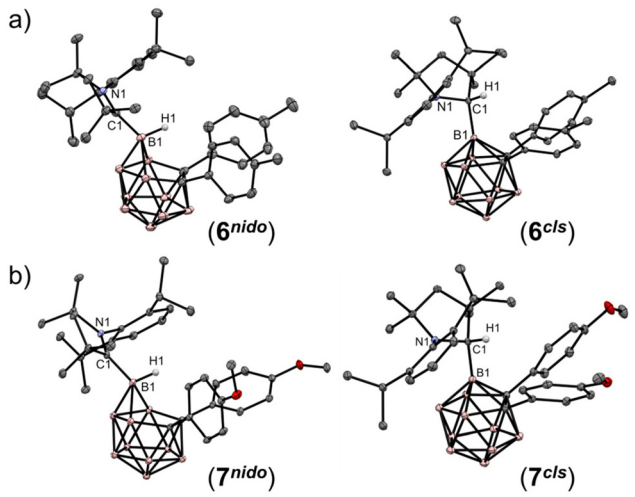

Fig. 11 (a) POV-ray depiction of 6^{nido} (left) and 6^{cls} (right). Thermal ellipsoids at 30% probability, and non-relevant hydrogen atoms are omitted for clarity; (b) POV-ray depiction of 7^{nido} (left) and 7^{cls} (right). Thermal ellipsoids at 30% probability, and non-relevant hydrogen atoms are omitted for clarity.

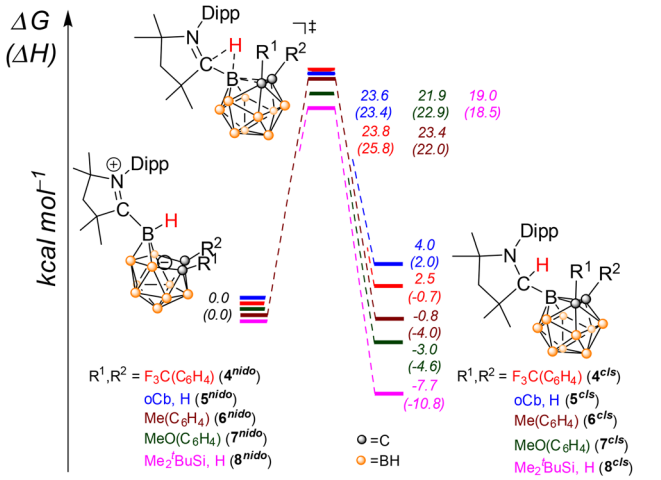

Fig. 12 DFT computed mechanism of the hydride migration from the boron to the carbon atom in ^{pCF3Ph2}***o*Cb**, ^{oCb}***o*Cb**, ^{pTol2}***o*Cb**, ^{Anis2}***o*Cb**, and ^{Si}**oCb**.

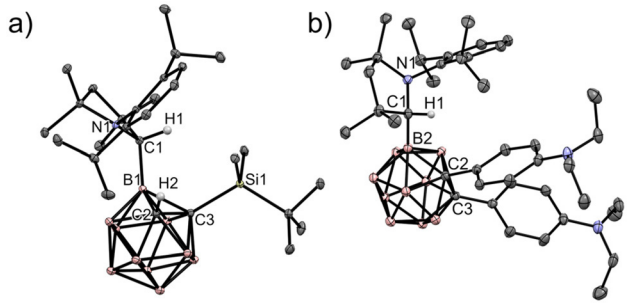

Fig. 13 POV-ray depiction of $\mathbf{8}^{cls}$ (a) and $\mathbf{9}^{cls}$ (b). Thermal ellipsoids at 30% probability, and non-relevant hydrogen atoms are omitted for clarity.

$\mathbf{9}^{cls}$ (Fig. 9, path f). Product $\mathbf{9}^{cls}$ was isolated by crystallization from hexane, and its X-ray molecular structure was determined using SC-XRD (Fig. 13b). Importantly, unlike in all other cases in which the insertion of the carbene into the B–H bond was observed at the most electrophilic B centre (B3), in this case, product $\mathbf{9}^{cls}$ clearly indicates that the ^{Me2}**CAAC** insertion into the B–H bond in ^{Anil2}***o*Cb** occurred at the B4 position. This could be explained by the steric hindrance that the *p*-Et_2N-C_6H_4 substituents create at positions B3 and B6.

We examined possible mechanisms for the formation of $\mathbf{9}^{cls}$ using DFT calculations (see the SI). Based on these computations, we propose that the reaction proceeds *via* initial attack of ^{Me2}**CAAC** at the B4 vertex of ^{Anil2}***o*Cb**, leading to a *nido*-type intermediate ($\mathbf{9}^{nido}$), followed by hydride migration and closure to afford $\mathbf{9}^{cls}$.

An alternative pathway involving insertion of ^{Me2}**CAAC** into the B3–H bond, followed by vertex migration (B3 to B4)[63] is also possible. However, according to our calculations, this route is overall slightly less favorable thermodynamically and kinetically.

Finally, to understand the reason behind the formation of the 2 : 1 product in the reaction of ^{Me2}**CAAC** with ^{Me2}***o*Cb** leading to $\mathbf{2}^{clscls}$ (see Fig. 3), we used DFT to compute the full reaction profile of this transformation at the B86-D3/def2SVP level of theory.[59–61] As a result, the reaction of ^{Me2}**CAAC** with ^{Me2}***o*Cb** leading to $\mathbf{2}^{nido}$ is strongly exothermic and exergonic (ΔH = −30.8 and ΔG = −15.2 kcal mol^{-1}), proceeding *via* **TS1** with the Gibbs free energy barrier of $\Delta G^{\ddagger}$ = 15.3 kcal mol^{-1}. The hydride migration in $\mathbf{2}^{nido}$ leading to $\mathbf{2}^{cls}$ is also exothermic and exergonic (ΔH = −14.9 and ΔG = −12.5 kcal mol^{-1}) with the Gibbs energy barrier (**TS2**) of $\Delta G^{\ddagger}$ = 19.4 kcal mol^{-1}, which is also the rate-determining step of this reaction. The attack of the second ^{Me2}**CAAC** on $\mathbf{2}^{cls}$ leading to $\mathbf{2}^{clsnido}$ is exothermic and exergonic (ΔH = −32.1 and ΔG = −17.3 kcal mol^{-1}) with an energy barrier of $\Delta G^{\ddagger}$ = 14.2 kcal mol^{-1}. The last step of the reaction is the hydride migration in $\mathbf{2}^{clsnido}$, leading to the final product $\mathbf{2}^{clscls}$, which is again highly

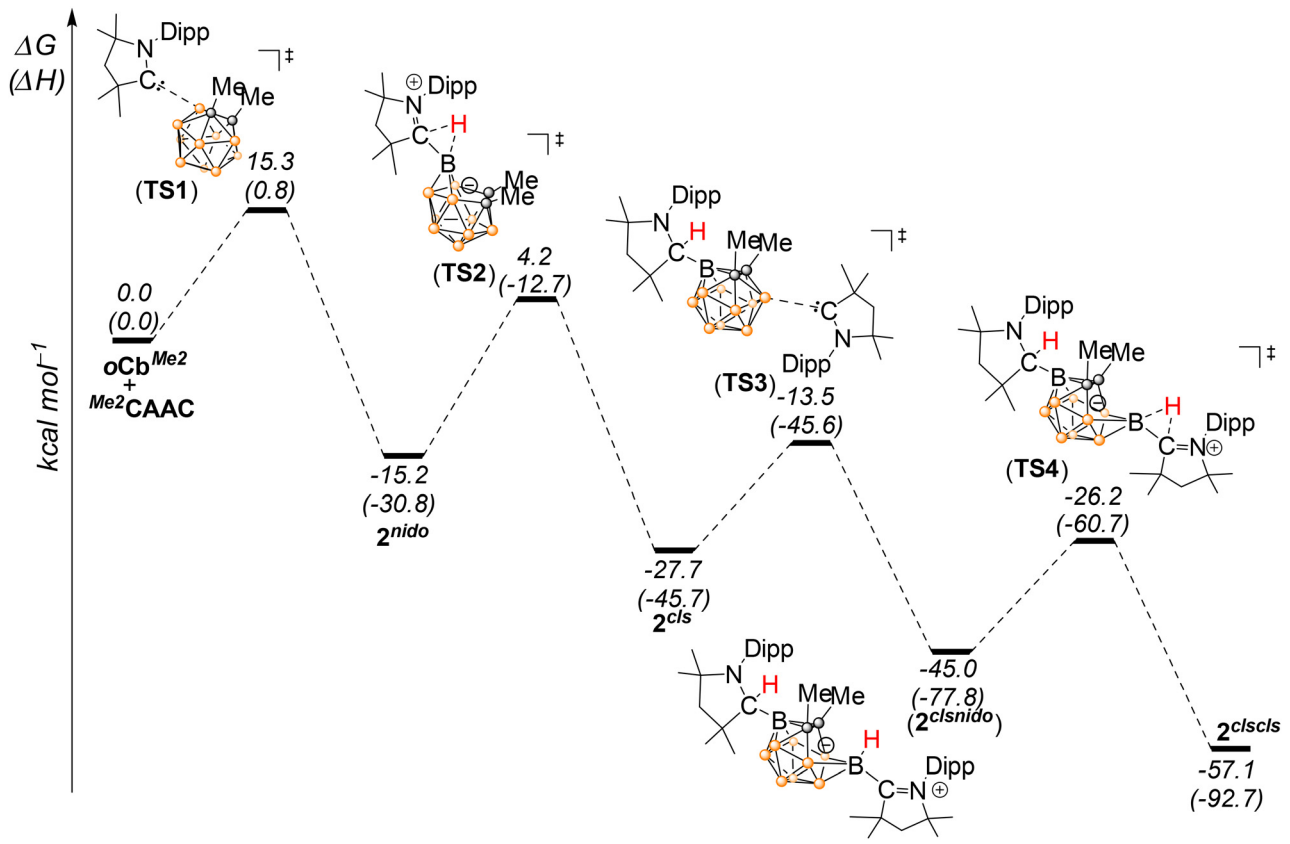

Fig. 14 DFT computed mechanism for the reaction between ^{Me2}***o*Cb** with ^{Me2}**CAAC** leading to the formation of $\mathbf{2}^{clscls}$.

exothermic and exergonic (ΔH = −14.9 and ΔG = −12.1 kcal mol^{-1}) with an energy barrier of $\Delta G^{\ddagger}$ = 18.8 kcal mol^{-1} (Fig. 14). From this computed reaction coordinate, it becomes evident that as soon as **2**^{cls} forms, it reacts directly with the second equivalent of ^{Me2}**CAAC** due to the lower Gibbs energy barriers of the following steps. This could be explained by the higher electrophilicity of the B6 centre in **2**^{cls} in comparison with ^{Me2}***o*Cb** due to the substitution of the ***o*Cb** cage by an electron-withdrawing cyclic amine. Importantly, these results can also explain why the 2 : 1 (^{Me2}**CAAC** : ^{R2}***o*Cb**) product was not obtained in all other cases. In addition to the steric factors that prevented the reaction of two molecules of ^{Me2}**CAAC** with different carboranes (^{R2}***o*Cb**), electronic factors affected these reactions in the following way: when the kinetic *nido* products were obtained as stable intermediates in 1 : 1 reactions, ^{Me2}**CAAC** was fully consumed, and therefore, 2 : 1 products were not obtained.

Conclusions

To conclude, in this work, the reactivity of ^{R2}***o*Cb**s was studied with ^{Me2}**CAAC**. The reaction of parent ***o*Cb** with ^{Me2}**CAAC** led to the insertion of the carbene into the C–H bond. When the carbons of the ***o*Cb** were substituted, the reaction of ^{Me2}**CAAC** took a different course that was guided by the nature of the substituents. Electron-withdrawing groups (EWGs) at the carbon centre(s) of ***o*Cb** led to *nido*-type carboranes as a result of the nucleophilic attack of ^{Me2}**CAAC** at the B3 (or B6) position. In contrast, electron-donating groups (EDGs) led to the insertion of the carbene into the B–H bond(s) at the B3 (or B6) position. Experimental and computational studies of the mechanism of these insertion processes revealed that this insertion proceeds *via nido* intermediates, by hydride migration from the B to C atom, and closing of the cluster. In the suggested mechanism, EWGs at the carbon centre stabilized the *nido* form and precluded the hydride migration and closing of the cluster; on the other hand, EDGs made the hydride transfer and closing of the cluster a favourable process. This study provided the first experimental evidence for the mechanism of nucleophilic substitution at B3 and/or B6 positions, as well as at the B4 (or B5) position in the case of large sterically encumbered substituents, and potentially will lead in the future to more controlled and selective substitution of ***o*Cb**s, as well as paving the way towards metal-free substitutions at these positions.

Conflicts of interest

There are no conflicts to declare.

Data availability

Data supporting this study are available in the supplementary information (SI). Supplementary information: NMR, MS, experimental and computational details (PDF). See DOI: https://doi.org/10.1039/d6qi00095a.

CCDC 2503802–2503813 and 2504008 contain the supplementary crystallographic data for this paper.[64a–m]

Acknowledgements

This work was supported by the Israeli Science Foundation, Grant 195/22, and the Israel Ministry of Science Technology & Space, Grant 01032376.

References

1 R. N. Grimes, Introduction and History, in *Carboranes*, Academic Press, 2nd edn, 2011, pp. 1–6.
2 X. Zhang, L. M. Rendina and M. Müllner, Carborane-Containing Polymers: Synthesis, Properties, and Applications, *ACS Polym. Au*, 2023, **4**, 7–33.
3 R. N. Grimes, Carboranes in medicine, in *Carboranes*, Academic Press, 2nd edn, 2011, pp. 1053–1082.
4 A. W. Tomich, J. Chen, V. Carta, J. Guo and V. Lavallo, Electrolyte Engineering with Carboranes for Next-Generation Mg Batteries, *ACS Cent. Sci.*, 2024, **10**, 264–271.
5 S. P. Fisher, A. W. Tomich, S. O. Lovera, J. F. Kleinsasser, J. Guo, M. J. Asay, H. M. Nelson and V. Lavallo, Nonclassical Applications of closo-Carborane Anions: From Main Group Chemistry and Catalysis to Energy Storage, *Chem. Rev.*, 2019, **119**, 8262–8290.
6 R. N. Grimes, Carboranes in catalysis, in *Carboranes*, Academic Press, 2nd edn, 2011, pp. 1037–1052.
7 D. Bawari, D. Toami, K. Jaiswal and R. Dobrovetsky, Hydrogen Splitting at a Single Phosphorus Centre and Its Use for Hydrogenation, *Nat. Chem.*, 2024, **16**, 1261–1266.
8 X. Tan, X. Wang, Z. H. Li and H. Wang, Borenium-Ion-Catalyzed C–H Borylation of Arenes, *J. Am. Chem. Soc.*, 2022, **144**, 23286–23291.
9 R. N. Grimes, Carboranes in other applications, in *Carboranes*, Academic Press, 2nd edn, 2011, pp. 1083–1105.
10 M. Keener, C. Hunt, T. G. Carroll, V. Kampel, R. Dobrovetsky, T. W. Hayton and G. Ménard, Redox-sitchable crboranes for uranium capture and release, *Nature*, 2020, **577**, 625–655.
11 R. N. Grimes, Metallacarboranes of the transition and lanthanide elements, in *Carboranes*, Academic Press, 2nd edn, 2011, pp. 773–1014.
12 D. J. Liston, Y. J. Lee, W. R. Scheidt and C. A. Reed, Observations on silver salt metathesis reactions with very weakly coordinating anions, *J. Am. Chem. Soc.*, 1989, **111**, 6643–6648.
13 C. A. Reed, Carboranes: A New Class of Weakly Coordinating Anions for Strong Electrophiles, Oxidants, and Superacids, *Acc. Chem. Res.*, 1998, **31**, 133–139.

14 R. N. Grimes, Icosahedral carboranes: 1,7-$C_2B_{10}H_{12}$ and 1,12-$C_2B_{10}H_{12}$, in *Carboranes*, Academic Press, 2nd edn, 2011, pp. 541–674.
15 A. D. Ready, V. Tej Raviprolu, T. A. Kerr, J. W. Treacy, M. L. Matsumoto, P. E. Hammer, E. M. Sletten, K. N. Houk and A. M. Spokoyny, Carboranes without Cage Carbons: closo-Dodecaborate Mimics of Neutral closo-Carboranes, *J. Am. Chem. Soc.*, 2025, **147**, 25478–25488.
16 R. N. Grimes, Structure and Bonding, in *Carboranes*, Academic Press, 2nd edn, 2011, pp. 7–20.
17 N. N. Greenwood and A. Earnshaw, Boron, in *Chemistry of the Elements*, Butterworth-Heinemann, 2nd edn, 1997, pp. 139–215.
18 V. I. Bregadze, Dicarba-closo-dodecaboranes $C_2B_{10}H_{12}$ and their derivatives, *Chem. Rev.*, 1992, **92**, 209–223.
19 Y. Quan and Z. Xie, Controlled functionalization of o-carborane via transition metal catalyzed B–H activation, *Chem. Soc. Rev.*, 2019, **48**, 3660–3673.
20 M. F. Hawthorne, D. C. Young, P. M. Garrett, D. A. Owen, S. G. Schwerin, F. N. Tebbe and P. A. Wegner, reparation and characterization of the (3)-1,2- and (3)-1,7-dicarbadodecahydroundecaborate(-1) ions, *J. Am. Chem. Soc.*, 1968, **90**, 862–868.
21 L. I. Zakharkin and V. N. Kalinin, On the Reaction of Amines with Barenes, *Tetrahedron Lett.*, 1965, **6**, 407–409.
22 R. A. Wiesboeck and M. F. Hawthorne, Dicarbaundecaborane(13) and Derivatives, *J. Am. Chem. Soc.*, 1964, **86**, 1642–1643.
23 H. D. A. C. Jayaweera, M. M. Rahman, P. J. Pellechia, M. D. Smith and D. V. Peryshkov, Free Three-dimensional Carborane Carbanions, *Chem. Sci.*, 2021, **12**, 10441–10447.
24 K. P. Anderson, H. A. Mills, C. Mao, K. O. Kirlikovali, J. C. Axtell, A. L. Rheingold and A. M. Spokoyny, Improved synthesis of icosahedral carboranes containing exopolyhedral B–C and C–C bonds, *Tetrahedron*, 2019, **75**, 187–191.
25 N. S. Hosmane, *Boron Science: New Technologies and Applications*, CRC Press, Boca Raton, 2011, pp. 3–20.
26 G.-X. Jin and Z. Xie, Carboranes Themed Issue, *Dalton Trans.*, 2014, **43**, 4924–5133.
27 V. I. Bregadze and Z. Xie, Boron Chemistry Themed Issue, *Eur. J. Inorg. Chem.*, 2017, 4344.
28 T. L. Chan and Z. Xie, Synthesis, structure and aromaticity of carborane-fused carbo- and heterocycles, *Chem. Sci.*, 2018, **9**, 2284–2289.
29 S. O. Lovera, A. Gregory, K. Espinoza Morelos, P. Farias, V. Carta, C. B. Musgrave III and V. Lavallo, Noncatalyzed Intramolecular B–N and B–O Cross-Coupling of "Inert" Carboranes Lead to the Formation of an Unusual Oxoborane, via Reversible Cluster C–B Bond Scission, *J. Am. Chem. Soc.*, 2025, **147**, 17764–17771.
30 C. Douvris and J. Michl, Chemistry of the Carbacloso-dodecaborate(−) Anion, $CB_{11}H_{12}^-$, *Chem. Rev.*, 2013, **113**, PR179–PR233.
31 Z. Zheng, W. Jiang, A. A. Zinn, C. B. Knobler and M. F. Hawthorne, Facile Electrophilic Iodination of Icosahedral Carboranes. Synthesis of Carborane Derivatives with Boron-Carbon Bonds via the Palladium-Catalyzed Reaction of Diiodocarboranes with Grignard Reagents, *Inorg. Chem.*, 1995, **34**, 2095–2100.
32 V. N. Lebedev, E. V. Balagurova, A. V. Polyakov, A. I. Yanovsky, Y. T. Struchkov and L. I. Zakharkin, Selective fluorination of o0 and m-carboranes. Synthesis of 9-monofluoro-, 9,12-difluoro-1,8,9,12-trifluoro-, and 8,9,10,12-tetrafluoro-o-carboranes and 9-monofluoro-, and 9,10-difluoro-m-carboranes. Molecular structure of 8,9,10,12-tetrafluoro-o-carborane, *J. Organomet. Chem.*, 1990, **385**, 307–318.
33 Y. Ma, H. Ren, Y. Wu, N. Li, F. Chen and X. Chen, B(9)-OH-o-Carboranes: Synthesis, Mechanism, and Property Exploration, *J. Am. Chem. Soc.*, 2023, **145**, 7331–7342.
34 F. Teixidor, G. Barberà, C. Viñas, R. Sillanpää and R. Kivekäs, Synthesis of Boron-Iodinated o-Carborane Derivatives. Water Stability of the Periodinated Monoprotic Salt, *Inorg. Chem.*, 2006, **45**, 3496–3498.
35 K. Wade, *Electron Deficient Compounds*, Springer, 1971.
36 R. Cheng, Z. Qiu and Z. Xie, Iridium-catalysed regioselective borylation of carboranes via direct B-H activation, *Nat. Commun.*, 2017, **8**, 14827.
37 Z. Qiu and Z. Xie, A Strategy for Selective Catalytic B–H Functionalization of o-Carboranes, *Acc. Chem. Res.*, 2021, **54**, 4065–4079.
38 M. Zhu, P. Wang, Z. Wu, Y. Zhong, L. Su, Y. Xin, A. M. Spokoyny, C. Zou and X. Mu, A Pd-catalyzed route to carborane-fused boron heterocycles, *Chem. Sci.*, 2024, **15**, 10392–10401.
39 Y. Quan and Z. Xie, Controlled functionalization of o-carborane via transition metal catalyzed B–H activation, *Chem. Soc. Rev.*, 2019, **48**, 3660–3673.
40 Z. Qiu, S. Ren and Z. Xie, Transition Metal-Carboryne Complexes: Synthesis, Bonding, and Reactivity, *Acc. Chem. Res.*, 2011, **44**, 299–309.
41 Y. Quan and Z. Xie, Palladium-Catalyzed Regioselective Diarylation of o-Carboranes By Direct Cage B–H Activation, *Angew. Chem., Int. Ed.*, 2016, **55**, 1295–1298.
42 R. Cheng, Z. Qiu and Z. Xie, Iridium–Catalyzed Regioselective B(3)–Alkenylation/B(3,6)–Dialkenylation of o–Carboranes by Direct B–H Activation, *Chem. – Eur. J.*, 2020, **26**, 7212–7218.
43 Y. Quan and Z. Xie, Iridium Catalyzed Regioselective Cage Boron Alkenylation of o-Carboranes via Direct Cage B–H Activation, *J. Am. Chem. Soc.*, 2014, **136**, 15513–15516.
44 C. Tang, J. Zhang, J. Zhang and Z. Xie, Regioselective Nucleophilic Alkylation/Arylation of B–H Bonds in o-Carboranes: An Alternative Method for Selective Cage Boron Functionalization, *J. Am. Chem. Soc.*, 2018, **140**, 16423–16427.
45 J. Zhang and Z. Xie, N-Ligand-Enabled, Aromatic Nucleophilic Amination of 1,2-Diaryl-o-Carboranes with $(R(_2)N)(_2)Mg$ for Selective Synthesis of 4-$R(_2)N$-o-Carboranes and 2-$R(_2)N$-m-Carboranes, *Angew. Chem., Int. Ed.*, 2022, **61**, e202202675.
46 M. Jones, W. Ando, M. E. Hendrick, A. Kulczycki, P. M. Howley, K. F. Hummel and D. S. Malament,

Irradiation of Methyl Diazomalonate in Solution. Reactions of Singlet and Triplet Carbenes with Carbon-Carbon Double Bonds, *J. Am. Chem. Soc.*, 1972, **94**, 7542–7549.

47 G.-X. Zheng and M. Jones, Reaction of (ethoxycarbonyl) carbene with o-carborane, *J. Am. Chem. Soc.*, 1983, **105**, 6487–6488.

48 K. Yuan and M. Jones, Carbenes Do React with p-Carborane, *Tetrahedron Lett.*, 1992, **33**, 7481–7484.

49 K. Lee, G. A. González-Montiel, H. Eom, T. H. Kim, H. C. Noh, A. O. Farah, H. R. Wise, D. Kim, P. H.-Y. Cheong and P. H. Lee, Site- and Enantioselective B–H Functionalization of Carboranes, *Nat. Commun.*, 2025, **16**, 4182.

50 N. Matsumi, Preparation of ionic liquids bearing o-carborane anion via N,N'-dialkylimidazol-2-ylidene carbene, *J. Organomet. Chem.*, 2009, **694**, 1612–1616.

51 C. E. Willans, C. A. Kilner and M. A. Fox, Deboronation and Deprotonation of ortho–Carborane with N–Heterocyclic Carbenes, *Chem. – Eur. J.*, 2010, **16**, 10644–10648.

52 F. Zheng and Z. Xie, Reaction of o-carboranes with sterically demanding N-heterocyclic carbene: synthesis and structural characterization of 1 : 1 adducts, *Dalton Trans.*, 2012, **41**, 12907–12914.

53 S. K. Kumar, A. Mishra, H. W. Roesky and K. C. Mondal, Recent Advances in the Domain of Cyclic (Alkyl)(Amino) Carbenes, *Chem. – Asian J.*, 2022, **17**, e202101301.

54 R. Jazzar, R. D. Dewhurst, J.-B. Bourg, B. Donnadieu, Y. Canac and G. Bertrand, Intramolecular "Hydroiminiumation" of Alkenes: Application to the Synthesis of Conjugate Acids of Cyclic Alkyl Amino Carbenes (CAACs), *Angew. Chem., Int. Ed.*, 2007, **46**, 2899–2902.

55 Y. Zhu, C. Li, M. Sudarmadji, H. M. Ng, B.-Y. Ao, J. A. Maguire and N. S. Hosmane, An efficient and recyclable catalytic system comprising nanopalladium(0) and a pyridinium salt of iron bis(dicarbollide) for oxidation of substituted benzyl alcohol and lignin, *ChemistryOpen*, 2012, **1**, 67–70.

56 P. W. Causey, T. R. Besanger and J. F. Valliant, Synthesis and Screening of Mono- and Di-Aryl Technetium and Rhenium Metallocarboranes. A New Class of Probes for the Estrogen Receptor, *J. Med. Chem.*, 2008, **51**, 2833–2844.

57 M. A. Fox, A. K. Hughes and J. M. Malget, Cage-closing reactions of the nido-carborane anion 7,9-$C_2B_9H_{12}^-$ and derivatives; formation of neutral 11-vertex carboranes by acidification, *J. Chem. Soc., Dalton Trans.*, 2002, 3505–3517.

58 T. D. McGrath, A. Franken, J. A. Kautz and F. G. A. Stone, Synthesis of nickel–monocarbollide complexes by oxidative insertion, *Inorg. Chem.*, 2005, **44**, 8135–8144.

59 J. P. Perdew, Density-functional approximation for the correlation energy of the inhomogeneous electron gas, *Phys. Rev. B: Condens. Matter Mater. Phys.*, 1986, **33**, 8822–8824.

60 A. D. Becke, Density-functional exchange-energy approximation with correct asymptotic behavior, *Phys. Rev. A*, 1988, **38**, 3098–3100.

61 F. Weigend and R. Ahlrichs, Balanced basis sets of split valence, triple zeta valence and quadruple zeta valence quality for H to Rn: Design and assessment of accuracy, *Phys. Chem. Chem. Phys.*, 2005, **7**, 3279–3305.

62 Y. O. Wong, M. D. Smith and D. V. Peryshkov, Cage Opening of a Carborane Ligand by Metal Cluster Complexes, *Chem. – Eur. J.*, 2016, **22**, 6764–6767.

63 S.-h. Wu and M. Jones Jr., The mechanism of rearrangement of the icosahedral carboranes, *J. Am. Chem. Soc.*, 1989, **111**, 5373–5384.

64 (*a*) CCDC 2503802: Experimental Crystal Structure Determination, 2026, DOI: **10.5517/ccdc.csd.cc2q1dt0**; (*b*) CCDC 2503803: Experimental Crystal Structure Determination, 2026, DOI: **10.5517/ccdc.csd.cc2q1dv1**; (*c*) CCDC 2503804: Experimental Crystal Structure Determination, 2026, DOI: **10.5517/ccdc.csd.cc2q1dw2**; (*d*) CCDC 2503805: Experimental Crystal Structure Determination, 2026, DOI: **10.5517/ccdc.csd.cc2q1dx3**; (*e*) CCDC 2503806: Experimental Crystal Structure Determination, 2026, DOI: **10.5517/ccdc.csd.cc2q1dy4**; (*f*) CCDC 2503807: Experimental Crystal Structure Determination, 2026, DOI: **10.5517/ccdc.csd.cc2q1dz5**; (*g*) CCDC 2503808: Experimental Crystal Structure Determination, 2026, DOI: **10.5517/ccdc.csd.cc2q1f07**; (*h*) CCDC 2503809: Experimental Crystal Structure Determination, 2026, DOI: **10.5517/ccdc.csd.cc2q1f18**; (*i*) CCDC 2503810: Experimental Crystal Structure Determination, 2026, DOI: **10.5517/ccdc.csd.cc2q1f29**; (*j*) CCDC 2503811: Experimental Crystal Structure Determination, 2026, DOI: **10.5517/ccdc.csd.cc2q1f3b**; (*k*) CCDC 2503812: Experimental Crystal Structure Determination, 2026, DOI: **10.5517/ccdc.csd.cc2q1f4c**; (*l*) CCDC 2503813: Experimental Crystal Structure Determination, 2026, DOI: **10.5517/ccdc.csd.cc2q1f5d**; (*m*) CCDC 2504008: Experimental Crystal Structure Determination, 2026, DOI: **10.5517/ccdc.csd.cc2q1mgw**.